Finite-size topology

Ashley M. Cook [1,2] and Anne E. B. Nielsen [3]
[1]*Max Planck Institute for Chemical Physics of Solids, Nöthnitzer Straße 40, 01187 Dresden, Germany*
[2]*Max Planck Institute for the Physics of Complex Systems, Nöthnitzer Straße 38, 01187 Dresden, Germany*
[3]*Department of Physics and Astronomy, Aarhus University, 8000 Aarhus C, Denmark*

(Received 19 April 2022; revised 21 December 2022; accepted 10 July 2023; published 28 July 2023)

We show that topological characterization and classification in D-dimensional systems, which are thermodynamically large in only $D-\delta$ dimensions and finite in size in δ dimensions, is fundamentally different from that of systems thermodynamically large in all D dimensions: As $(D-\delta)$-dimensional topological boundary states permeate into a system's D-dimensional bulk with decreasing system size, they hybridize to create novel topological phases characterized by a set of $\delta+1$ topological invariants, ranging from the D-dimensional topological invariant to the $(D-\delta)$-dimensional topological invariant. The system exhibits topological response signatures and bulk-boundary correspondences governed by combinations of these topological invariants taking nontrivial values, with lower-dimensional topological invariants characterizing fragmentation of the underlying topological phase of the system thermodynamically large in all D dimensions. We demonstrate this physics for the paradigmatic Chern insulator phase, but show its requirements for realization are satisfied by a much broader set of topological systems.

DOI: 10.1103/PhysRevB.108.045144

Consequences of topology in condensed-matter physics frequently stem from the nontrivial topological invariant of a material bulk associated with incompressible states, corresponding to topological response signatures of the bulk and topologically protected boundary states [1–3]. These signatures yield the unpaired Majorana zero modes required for topological quantum computation [4–11] and topological boundary metals useful for spintronics devices [12–19], for instance, reflecting their significance. While the relationship between bulk topological responses and topological boundary states has typically been studied in systems large enough that finite-size effects are neglected while still yielding good agreement with experiment [20–22], significant improvements in fabrication techniques now permit experimental study of lower-dimensional systems in which finite-size effects are significant. Past work on such systems has reported findings of lower-dimensional topological phases [23–30] or higher-dimensional phases [27,31–37] rather than the transition from higher-dimensional to lower-dimensional topological phases itself, motivating greater scrutiny of this process.

We address the need for greater understanding of this transition between higher-dimensional and lower-dimensional topological phases by showing that finite-size effects can yield *additional, previously unidentified topological phases*. In the case of the Chern insulator, which is two-dimensional (2D) in the bulk, we consider opening boundary conditions in one direction and thinning the system in this direction to a quasi-one-dimensional geometry, which we denote as quasi-(2-1)D as the underlying bulk is 2D. While dimensional reduction also considers opening boundary conditions in one direction and thinning the system in one direction, the system size is large in the direction in which boundary conditions are opened, and it is small in the periodic direction [38]. Dimensional reduction also holds even when the system is thinned to be strictly one-dimensional. We note that this scenario considered for dimensional reduction, of system size large in the direction of open boundary conditions, is also the regime considered by the tenfold way classification scheme [20]. We instead consider thinning the system in the direction in which boundary conditions are opened, to finite thicknesses that are small relative to the penetration depth of topological boundary modes, and keeping the system size thermodynamically large in the periodic direction.

We also report on effects here which only occur for systems finite in width in the direction of open boundary conditions. In this case, the quasi-(2-1)D Chern insulator can still exhibit charge pumping in response to changing magnetic flux through a plaquette of the lattice due to a nontrivial Chern number. However, if we open boundary conditions in the second direction, the quasi-(2-1)D Chern insulator also exhibits a second bulk-boundary correspondence, with quasi-zero-dimensional—or quasi-(2-2)D—topologically protected, gapless boundary modes localized at the ends of the quasi-(2-1)D system, in correspondence with a lower-dimensional topological invariant characterizing topology of the quasi-(2-1)D bulk. These quasi-zero-dimensional states are topologically robust and cannot be understood purely through interference of chiral modes. Furthermore, the number of topologically

robust quasi-zero-dimensional modes at each end of the ribbon can be integer-valued in direct correspondence with the Chern number, in the presence of only a $\sigma_z\mathcal{I}$ symmetry. This symmetry may be interpreted as spatial inversion symmetry depending upon the choice of physical degrees of freedom, but this integer classification indicates that $\mathbb{Z}_2$ topological invariants of 1D topological insulators protected by spatial inversion symmetry are therefore unsuitable [39]. Instead, $\mathbb{Z}$ classification indicates previously unidentified topological phases characterized by both a $\mathbb{Z}$ Chern number and a related $\mathbb{Z}$ lower-dimensional topological invariant. As topological phases are defined by their topological invariant(s) [20,22,40], the characterization of topological states of finite-size systems in terms of a set of topological invariants of different dimensionalities—and in terms of more topological invariants than required for D-dimensional systems which are thermodynamically large in all D dimensions—is fundamentally different from previous work.

We consider finite-size topological phases here for systems with a $\sigma_z\mathcal{I}$ symmetry, where $\mathcal{I}$ is lattice inversion and σ_z acts on the orbital space and squares to the identity. Our results are therefore broadly applicable to topological phases irrespective of other symmetries present and bulk dimensionality, in particular, given the Chern insulator phase is used to construct many other topological phases of matter [3,19,41–48]. We expect finite-size topological phases to be prominent in lower-dimensional materials with nontrivial topology such as stacked van der Waals materials and nanowires.

Finite-size topology of the Chern insulator. We first show that finite-size topology occurs in the 2D Chern insulator phase. The phase is foundational both in understanding the quantum anomalous Hall effect [49] and as a building block used to construct many other topological phases of matter, most notably the quantum spin Hall insulator [19,50], the three-dimensional topological insulator [42], and the Weyl semimetal [51,52]. Various analogs of the Chern insulator that are not electronic [53,54] and/or out of equilibrium [55,56] are also expected to display finite-size topology.

The considered Chern insulator Hamiltonian,

$$\begin{aligned} H_{\mathrm{CI}} = &\sum_{\sigma,n,m} \sigma(M+\kappa_{n,m}) c^\dagger_{\sigma,n,m} c_{\sigma,n,m} \\ &- t\sum_{\sigma,n,m} [\sigma c^\dagger_{\sigma,n,m} c_{\sigma,n+1,m} + (\sigma - \epsilon) c^\dagger_{\sigma,n,m} c_{\sigma,n,m+1} + \mathrm{H.c.}] \\ &- \Delta \sum_{\sigma,n,m} (\sigma c^\dagger_{\sigma,n,m} c_{-\sigma,n+1,m} + i c^\dagger_{\sigma,n,m} c_{-\sigma,n,m+1} + \mathrm{H.c.}), \end{aligned} \tag{1}$$

is a simplified version of the Qi-Wu-Zhang model [57] on an $L_x \times L_y$ square lattice, where $c^\dagger_{\sigma,n,m}$ creates a particle in the orbital $\sigma \in \{-1, 1\}$ at the site position (n, m), M is the Zeeman field strength, t is the strength of real hopping in both $\hat{x}$ and $\hat{y}$ directions without changing the orbital, and Δ is the strength of the hopping term changing the orbital. For $\epsilon = 0$ this Hamiltonian has a particle-hole symmetry described by the operator $\sigma_x K$, and for $\kappa_{n,m} = 0$ it has $\sigma_z\mathcal{I}$ symmetry. Here, σ_x and σ_z are Pauli matrices acting on the orbital space, K is the complex conjugation, and $\mathcal{I}$ is the inversion of the 2D lattice. Unless specified otherwise, we take $t = 1$, $\Delta = 0.22$, $\epsilon = \kappa_{n,m} = 0$, and $L_y = 600$ in the numerical computations below. For these parameters, the Hamiltonian realizes a Chern insulator phase with the Chern number $\mathcal{C} = +1$ for $-4 < M < 0$ and a distinct Chern insulator phase with the Chern number $\mathcal{C} = -1$ for $0 < M < 4$. In the following, we use (pe,pe), (op,pe), and (op,op) to refer to different combinations of open (op) and periodic (pe) boundary conditions in the $\hat{x}$ and $\hat{y}$ directions.

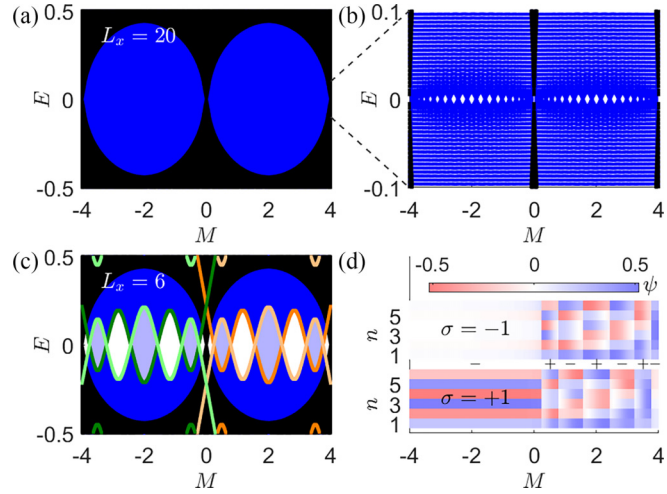

FIG. 1. (a) The single-particle energy spectrum E of the considered Chern insulator model on a 20×600 square lattice with (pe,pe) boundary conditions (black) is gapped except at a few values of the Zeeman field strength M. The spectrum for (op,pe) boundary conditions (blue) has states inside this gap. (b) When zooming panel (a) to a smaller energy range, small gaps in the (op,pe) spectrum become discernible. (c) When L_x is decreased, the small gaps become larger. Eigenstates in the (op,pe) spectrum with momentum $k_y = 0$ ($k_y = \pi$) are highlighted by their $\sigma_z\mathcal{I}$ eigenvalue [light orange (green) for $+1$ eigenvalue and dark orange (green) for -1 eigenvalue]. Intervals in M over which the highest-energy occupied state at half filling within the $k_y = 0$ and $k_y = \pi$ sectors have opposite $\sigma_z\mathcal{I}$ eigenvalues are highlighted with purple background color. (d) Components of the highest-energy occupied state within the $k_y = 0$ sector versus M for $L_x = 6$ and (op,pe) boundary conditions. The wave function is real, and the components are labeled by orbital σ and unit cell position n in the $\hat{x}$ direction. The $\sigma_z\mathcal{I}$ eigenvalues are indicated with plus and minus signs.

For a gapped topological phase characterized in a 2D bulk by a nontrivial Chern number $\mathcal{C}$, we generally expect $\mathcal{C}$ chiral modes localized on each edge if the boundary conditions are opened in one direction $\hat{x}$ and the system size in the $\hat{x}$ direction, L_x, is sufficiently large. The edge modes give rise to the blue states inside the 2D bulk energy gap seen in Fig. 1(a). As L_x is decreased, however, the system becomes quasi-(2-1)D. The states appearing within the 2D bulk energy gap increasingly permeate into the quasi-(2-1)D bulk and hybridize, such that we can only refer to them as states within the 2D bulk gap resulting from bulk-boundary correspondence, rather than edge states. The hybridization among these states can produce gaps in the quasi-(2-1)D spectrum. In fact, small gaps can already be seen for $L_x = 20$ [Fig. 1(b)], but the effect is much larger for smaller L_x [Fig. 1(c)]. When viewed as a function of a parameter of the model, the gaps can form bubbles separated

by transition points as seen in Fig. 1(c). A general mechanism to obtain such bubbles is when the highest-energy occupied state and lowest-energy unoccupied state of the quasi-(2-1)D bulk belong to different symmetry sectors and oscillate out of phase with sufficiently large amplitude as a function of the considered parameter. We describe below how this happens for the Chern insulator. For the quasi-(2-1)D Chern insulator, we find that there are $2L_x$ transition points and, hence, $2L_x - 1$ bubbles.

We first consider the case $\kappa_{n,m} = \epsilon = 0$. If $|\psi\rangle$ is an eigenstate of $H_{\rm CI}$ with energy E and an eigenstate of $\sigma_z\mathcal{I}$ with the eigenvalue s, then $\sigma_x K|\psi\rangle$ is an eigenstate of $H_{\rm CI}$ with the energy $-E$ and an eigenstate of $\sigma_z\mathcal{I}$ with the eigenvalue $-s$. Nondegenerate pairs of states with energies $\pm E$ hence have opposite $\sigma_z\mathcal{I}$ eigenvalues. Note also that $H_{\rm CI}$ and $\sigma_z\mathcal{I}$ can be simultaneously diagonalized within the sector with the momentum $k_y = 0$ in the $\hat{y}$ direction. The $\sigma = +1$ component of the resulting eigenstates is symmetric (antisymmetric) under the mirror operation that takes site n into $L_x + 1 - n$ if the $\sigma_z\mathcal{I}$ eigenvalue is $+1$ (-1) while the $\sigma = -1$ component is antisymmetric (symmetric). Similar considerations apply for $k_y = \pi$.

We observe numerically [Fig. 1(c)] that the lowest-energy unoccupied state and the highest-energy occupied state forming the $L_x - 1$ bubbles at $M > 0$ have the momentum $k_y = 0$. Plotting the highest-energy occupied state at half filling within the $k_y = 0$ sector [Fig. 1(d)], we observe that the wavelength of the wave function in the $\hat{x}$ direction decreases as M goes from 4 to 0. Let us consider the $\sigma = -1$ components of the state. The global phase of the wave function is chosen such that the component at $n = 1$ is positive. For symmetric (antisymmetric) states, the component at $n = L_x$ is hence positive (negative). A smoother change in the wavelength as a function of M can hence be obtained by alternating between symmetric and antisymmetric states, and this alternation produces the bubbles. The alternating sign of the $\sigma_z\mathcal{I}$ eigenvalue for the highest-energy occupied state also means that the product of $\sigma_z\mathcal{I}$ eigenvalues over high-symmetry points in the slab Brillouin zone undergoes a relative change in sign when tuning M through a transition point between two bubbles. The transition points therefore generically correspond to topological phase transitions.

We may further characterize the topology of the bubbles as topologically nontrivial or trivial by considering half filling and computing the eigenvalue spectrum of the (discretized) Wilson loop operator [59]

$$W_{jk} = \lim_{S\to\infty} \langle \psi_0^{(j)} | P_{S-1} P_{S-2} \cdots P_2 P_1 | \psi_0^{(k)} \rangle, \qquad (2)$$

where $|\psi_0^{(j)}\rangle$ is the jth occupied energy eigenstate within the $k_y = 0$ sector and P_l is the projector onto the occupied subspace within the $k_y = 2\pi l/S$ momentum sector. The eigenvalues of W_{jk} are phase factors $\{e^{i\vartheta^{(j)}}\}$, and the model is topological if at least one of the Wannier charge centers $\{\vartheta^{(j)}\}$ is $\pm\pi$. Such characterization of the quasi-(2-1)D bulk topology is depicted in Fig. 2(a).

We observe numerically that the highest-energy occupied state as a function of k_y is separated from the remaining occupied states (see Supplemental Material [58], Sec. I), and hence, we can also compute the Wannier charge center for this state alone. For systems with inversion symmetry, one can determine the number of Wannier charge centers that are $\pm\pi$ from the inversion eigenvalues at the momenta $k_y = 0$ and $k_y = \pi$ [59]. This explains the agreement between the purple regions in Figs. 2(a) and 1(c).

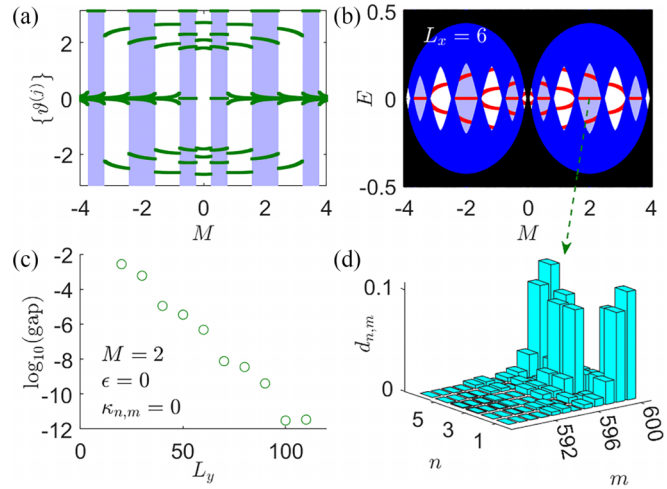

FIG. 2. 1D topology in the quasi-(2-1)D system. (a) Wannier spectrum versus Zeeman field strength M for (op,pe) boundary conditions and $L_x = 6$. Intervals in M, for which one of the Wannier charge centers is $\pm\pi$, are highlighted in purple. (b) Results of Fig. 1(c) for (pe,pe) and (op,pe) boundary conditions superimposed over the corresponding (op,op) spectrum (red). (c) The energy gap between the nearly degenerate in-gap states at zero energy in the (op,op) spectrum decreases exponentially with L_y, with variations due to Friedel oscillations. (d) Density distribution $d_{n,m} = \sum_\sigma \langle c^\dagger_{\sigma,n,m} c_{\sigma,n,m}\rangle$ of one of the two states at zero energy in the quasi-(2-1)D bulk gap for (op,op) boundary conditions and $M = 2$. We show only the outermost 12 rows of sites for the slab as more than 99.8% of the total density is located here. The other state is localized at the other end.

There is *an additional bulk-boundary correspondence* of the quasi-(2-1)D Chern insulator when the Wilson loop spectrum possesses topologically nontrivial eigenvalues: When M lies inside an interval corresponding to a topological bubble for open boundary conditions in the $\hat{x}$ direction and finite L_x, additionally opening boundary conditions in the $\hat{y}$ direction yields a pair of topological, quasi-(2-2)D gapless boundary modes at zero energy inside the bubble [Fig. 2(b)]. The energy gap between these two states displays exponential decay to zero with increasing L_y [Fig. 2(c)], and the probability density of one of these states for (op,op) boundary conditions is shown in Fig. 2(d). The probability density is strongly localized at one end of the system in the $\hat{y}$ direction, such that it is quasi-0D. As the system with (pe,pe) boundary conditions is two-dimensional, we more precisely identify these states as quasi-(2-2)D. The finite-size topology in the Chern insulator has $\mathbb{Z}$ topological classification, as discussed in the Supplemental Material [58], Sec. IV.

While there are additional states at nonzero energy in the bubbles for the parameter sets shown and they are localized and robust against disorder while in the bubble gap, these states are consumed by the quasi-(2-1)D bulk through smooth deformation of the system that reduces the maximum height

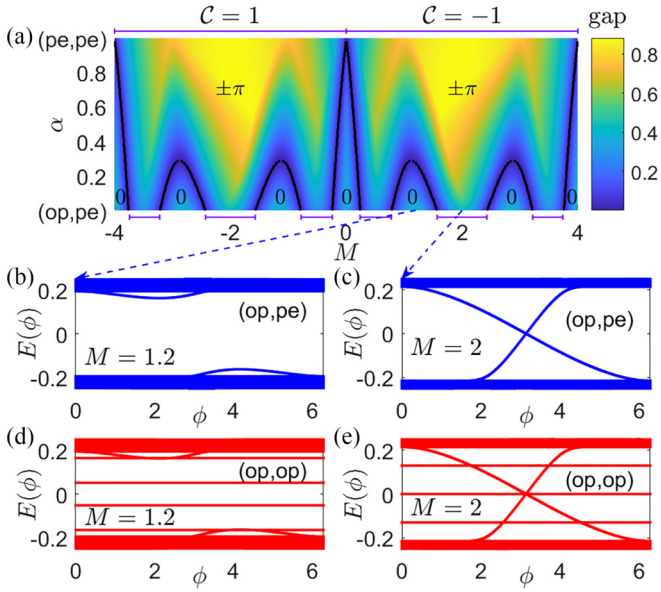

FIG. 3. Two-dimensional topological response in the quasi-(2-1)D system. (a) We continuously open the boundary conditions in the $\hat{x}$ direction by scaling the hopping strengths of all hops across the boundary by α. In this process, gap closings happen for some M but not for others. The regions where gap closings do not occur remain topological. The black lines that fall on top of the gap closings are the boundaries between topological regions in which the Wannier charge center of the highest-energy occupied state is $\pm\pi$ and trivial regions in which it is 0. The purple line segments above and below the plot show the topological regions for (pe,pe) and (op,pe) boundary conditions, respectively. (b,c) When inserting a flux ϕ through the central plaquette of the 6×600 lattice, the single-particle spectrum of the Chern insulator model shows (b) no pumping inside trivial bubbles and (c) Thouless pumping inside topological bubbles across the gap in the (op,pe) spectrum. (d,e) The in-gap states for (op,op) boundary conditions are not affected by the flux insertion, as they are localized at the ends of the slab.

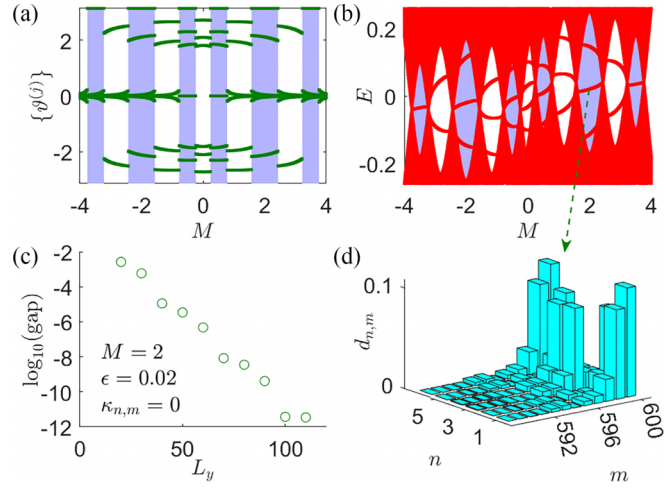

FIG. 4. (a) Wannier spectrum versus Zeeman field strength M when particle-hole symmetry is broken by taking $\epsilon = 0.02$. M intervals for which at least one Wannier charge center is $\pm\pi$ are highlighted in purple. (b) Single-particle spectrum for (op,op) boundary conditions (red) of the Chern insulator slab with $L_x = 6$, $L_y = 600$, $\epsilon = 0.02$, and $\kappa = 0.02$ averaged over 200 disorder realizations (see Supplemental Material [58], Sec. III, for details of disorder treatment). The in-gap states are twofold degenerate, and the purple background shows the topological regions computed for $\kappa = 0$. (c) The energy gap between the nearly degenerate, quasi-(2-2)D boundary modes (states L_xL_y and $L_xL_y + 1$) for $M = 2$, $\epsilon = 0.02$, and $\kappa = 0$ decreases exponentially with L_y. (d) The quasi-(2-2)D nature of the boundary modes inside the bubble gaps is manifested in the density distributions $d_{n,m} = \sum_\sigma \langle c^\dagger_{\sigma,n,m} c_{\sigma,n,m} \rangle$ of the states, here plotted for $M = 2$, $\epsilon = 0.02$, $\kappa = 0.02$, and one disorder realization. We show only the outermost 12 rows of sites for the slab as more than 99.8% of the total density is located here. The other state is localized at the other end. We obtain similar results for $L_x = 5$ (see Supplemental Material, Secs. II and III).

of the bubbles in energy. The quasi-(2-2)D states at nearly zero energy, in contrast, occur in correspondence with the nontrivial Wilson loop spectrum of these bubbles and are only removed by closing the quasi-(2-1)D bulk gap.

In addition to the bulk-boundary correspondence between a topological invariant of the quasi-(2-1)D bulk and quasi-(2-2)D topologically protected boundary states, however, the finite-size topology Chern insulator is adiabatically connected to a 2D system with a nonzero Chern number [Fig. 3(a)], and response signatures of this topology persist in the quasi-(2-1)D system, clearly distinguishing a quasi-(2-1)D finite-size topological phase from a 1D topological phase. This is demonstrated by computing the evolution of the spectrum for the quasi-1D Chern insulator with open boundary conditions in each direction, as a function of the magnetic flux ϕ through the center plaquette of the lattice [Figs. 3(b)–(e)]. Such ϕ dependence of the energy spectrum results from the dependence of the charge density on the applied magnetic field strength determined by the Chern number [60]. We find such charge pumping in the spectrum versus ϕ, but *only for topologically nontrivial bubbles*. Notably, the quasi-(2-2)D boundary states remain at fixed energy while ϕ is varied, reflecting their dependence on the topologically nontrivial polarization invariant of the quasi-(2-1)D bulk rather than on the full Chern number.

We also consider the Chern insulator with a finite-width wire geometry in the case of the particle-hole symmetry-breaking term ϵ being nonzero. Also in this case, we observe topological and trivial bubbles in the spectrum as a function of M characterized by quantized Wilson loop eigenvalues [Fig. 4(a)] and pairs of degenerate quasi-(2-2)D in-gap states localized at the ends of the wire [Fig. 4(c)]. We also observe flux pumping similar to the results in Fig. 3. If we add disorder of the strength $\kappa = 0.02$ by randomly choosing $\kappa_{n,m} \in [-\kappa, \kappa]$, both the momentum and the $\sigma_z\mathcal{I}$ symmetry are broken. The (op,op) spectrum still shows bubbles with in-gap states as a function of M. The in-gap states are localized at the ends of the wire [Fig. 4(d)], but there is now an energy gap between pairs of in-gap states with densities at opposite ends. If the spectrum is averaged over several disorder realizations, however, this gap averages to zero [Fig. 4(b) and Supplemental Material, Sec. III].

Conclusion. We show D-dimensional topological phases exhibit additional nontrivial *finite-size* topology: Topologically protected $(D-1)$-dimensional boundary modes

resulting from nontrivial topology of a D-dimensional bulk can hybridize in finite-size systems to induce additional topological phase transitions in the finite D-dimensional system with open boundary conditions *even when the D-dimensional bulk gap remains open*. This additional nontrivial topology in the finite-size D-dimensional system can yield an additional bulk-boundary correspondence to realize additional topologically protected quasi-(D-2)-dimensional boundary states, while the system still exhibits the response theory of a D-dimensional topological invariant. We show such finite-size topology occurs in Chern insulators, realizing quasi-(2-2)D topological modes in a quasi-(2-1)D system and charge pumping in response to an applied magnetic field. As Chern insulators are the basis for many other models and topological phases [3,19,41–48], such finite-size topology is a generic property that necessitates reexamination of known topological phases, to be explored in future work.

Acknowledgments. We thank Joel E. Moore for helpful discussions. This work has been supported by Danmarks Frie Forskningsfond under Grant No. 8049-00074B and Carlsbergfondet under Grant No. CF20-0658. This research was also supported in part by the National Science Foundation under Grant No. NSF PHY-1748958.

A.M.C. developed the concept. A.M.C. and A.E.B.N. performed the calculations, interpreted the results, and wrote the manuscript.

[1] R. B. Laughlin, Quantized Hall conductivity in two dimensions, Phys. Rev. B **23**, 5632 (1981).

[2] B. I. Halperin, Quantized Hall conductance, current-carrying edge states, and the existence of extended states in a two-dimensional disordered potential, Phys. Rev. B **25**, 2185 (1982).

[3] M. Z. Hasan and J. E. Moore, Three-dimensional topological insulators, Annu. Rev. Condens. Matter Phys. **2**, 55 (2011).

[4] A. Y. Kitaev, Unpaired Majorana fermions in quantum wires, Phys.-Usp. **44**, 131 (2001).

[5] N. Read and D. Green, Paired states of fermions in two dimensions with breaking of parity and time-reversal symmetries and the fractional quantum Hall effect, Phys. Rev. B **61**, 10267 (2000).

[6] T. D. Ladd, F. Jelezko, R. Laflamme, Y. Nakamura, C. Monroe, and J. L. O'Brien, Quantum computers, Nature (London) **464**, 45 (2010).

[7] R. Raussendorf and J. Harrington, Fault-Tolerant Quantum Computation with High Threshold in Two Dimensions, Phys. Rev. Lett. **98**, 190504 (2007).

[8] M. H. Freedman, A. Kitaev, M. J. Larsen, and Z. Wang, Topological quantum computation, Bull. Amer. Math. Soc. **40**, 31 (2003).

[9] C. Nayak, S. H. Simon, A. Stern, M. Freedman, and S. Das Sarma, Non-Abelian anyons and topological quantum computation, Rev. Mod. Phys. **80**, 1083 (2008).

[10] A. Kitaev, Fault-tolerant quantum computation by anyons, Ann. Phys. **303**, 2 (2003).

[11] J. Alicea and P. Fendley, Topological phases with parafermions: Theory and blueprints, Annu. Rev. Condens. Matter Phys. **7**, 119 (2016).

[12] M. N. Baibich, J. M. Broto, A. Fert, F. Nguyen Van Dau, F. Petroff, P. Etienne, G. Creuzet, A. Friederich, and J. Chazelas, Giant Magnetoresistance of (001)Fe/(001)Cr Magnetic Superlattices, Phys. Rev. Lett. **61**, 2472 (1988).

[13] G. Binasch, P. Grünberg, F. Saurenbach, and W. Zinn, Enhanced magnetoresistance in layered magnetic structures with antiferromagnetic interlayer exchange, Phys. Rev. B **39**, 4828 (1989).

[14] S. Murakami, N. Nagaosa, and S.-C. Zhang, Dissipationless quantum spin current at room temperature, Science **301**, 1348 (2003).

[15] J. Sinova, D. Culcer, Q. Niu, N. A. Sinitsyn, T. Jungwirth, and A. H. MacDonald, Universal Intrinsic Spin Hall Effect, Phys. Rev. Lett. **92**, 126603 (2004).

[16] M. König, H. Buhmann, L. W. Molenkamp, T. Hughes, C.-X. Liu, X.-L. Qi, and S.-C. Zhang, The quantum spin Hall effect: Theory and experiment, J. Phys. Soc. Jpn. **77**, 031007 (2008).

[17] E. Lesne, Y. Fu, S. Oyarzun, J. C. Rojas-Sánchez, D. C. Vaz, H. Naganuma, G. Sicoli, J. P. Attané, M. Jamet, E. Jacquet, J. M. George, A. Barthélémy, H. Jaffrès, A. Fert, M. Bibes, and L. Vila, Highly efficient and tunable spin-to-charge conversion through Rashba coupling at oxide interfaces, Nat. Mater. **15**, 1261 (2016).

[18] K. Kondou, R. Yoshimi, A. Tsukazaki, Y. Fukuma, J. Matsuno, K. S. Takahashi, M. Kawasaki, Y. Tokura, and Y. Otani, Fermi-level-dependent charge-to-spin current conversion by Dirac surface states of topological insulators, Nat. Phys. **12**, 1027 (2016).

[19] B. A. Bernevig, T. L. Hughes, and S.-C. Zhang, Quantum spin Hall effect and topological phase transition in HgTe quantum wells, Science **314**, 1757 (2006).

[20] S. Ryu, A. P. Schnyder, A. Furusaki, and A. W. W. Ludwig, Topological insulators and superconductors: Tenfold way and dimensional hierarchy, New J. Phys. **12**, 065010 (2010).

[21] C.-K. Chiu, J. C. Y. Teo, A. P. Schnyder, and S. Ryu, Classification of topological quantum matter with symmetries, Rev. Mod. Phys. **88**, 035005 (2016).

[22] A. P. Schnyder, S. Ryu, A. Furusaki, and A. W. W. Ludwig, Classification of topological insulators and superconductors in three spatial dimensions, Phys. Rev. B **78**, 195125 (2008).

[23] A. C. Potter and P. A. Lee, Multichannel Generalization of Kitaev's Majorana End States and a Practical Route to Realize Them in Thin Films, Phys. Rev. Lett. **105**, 227003 (2010).

[24] M. M. Asmar, D. E. Sheehy, and I. Vekhter, Topological phases of topological-insulator thin films, Phys. Rev. B **97**, 075419 (2018).

[25] Q. L. He, G. Yin, L. Yu, A. J. Grutter, L. Pan, C.-Z. Chen, X. Che, G. Yu, B. Zhang, Q. Shao, A. L. Stern, B. Casas, J. Xia, X. Han, B. J. Kirby, R. K. Lake, K. T. Law, and K. L. Wang, Topological Transitions Induced by Antiferromagnetism in a Thin-Film Topological Insulator, Phys. Rev. Lett. **121**, 096802 (2018).

[26] M. M. Otrokov, I. P. Rusinov, M. Blanco-Rey, M. Hoffmann, A. Y. Vyazovskaya, S. V. Eremeev, A. Ernst, P. M. Echenique, A. Arnau, and E. V. Chulkov, Unique Thickness-Dependent Properties of the van der Waals Interlayer Antiferromagnet $MnBi_2Te_4$ Films, Phys. Rev. Lett. **122**, 107202 (2019).

[27] S. Chowdhury, K. F. Garrity, and F. Tavazza, Prediction of Weyl semimetal and antiferromagnetic topological insulator phases in Bi_2MnSe_4, npj Comput. Mater. **5**, 33 (2019).

[28] J. Li, Y. Li, S. Du, Z. Wang, B.-L. Gu, S.-C. Zhang, K. He, W. Duan, and Y. Xu, Intrinsic magnetic topological insulators in van der Waals layered $MnBi_2Te_4$-family materials, Sci. Adv. **5** (2019).

[29] C. Lei, S. Chen, and A. H. MacDonald, Magnetized topological insulator multilayers, Proc. Natl. Acad. Sci. USA **117**, 27224 (2020).

[30] J. Liu and T. Hesjedal, Magnetic topological insulator heterostructures: A review, Adv. Mater. **35**, 2102427 (2021).

[31] Y. Gong, J. Guo, J. Li, K. Zhu, M. Liao, X. Liu, Q. Zhang, L. Gu, L. Tang, X. Feng, D. Zhang, W. Li, C. Song, L. Wang, P. Yu, X. Chen, Y. Wang, H. Yao, W. Duan, Y. Xu *et al.*, Experimental realization of an intrinsic magnetic topological insulator, Chin. Phys. Lett. **36**, 076801 (2019).

[32] B. Irfan, Surface characterization and magneto-transport study on Bi_2Te_2Se topological insulator thin film, Appl. Phys. A **126**, 191 (2020).

[33] M. Mir and S. H. Abedinpour, Dynamical density response and collective modes of topological-insulator ultrathin films, Phys. Rev. B **101**, 115108 (2020).

[34] P. Thalmeier and A. Akbari, Gapped Dirac cones and spin texture in thin film topological insulator, Phys. Rev. Res. **2**, 033002 (2020).

[35] L. Xu, Y. Mao, H. Wang, J. Li, Y. Chen, Y. Xia, Y. Li, D. Pei, J. Zhang, H. Zheng, K. Huang, C. Zhang, S. Cui, A. Liang, W. Xia, H. Su, S. Jung, C. Cacho, M. Wang, G. Li *et al.*, Persistent surface states with diminishing gap in $MnBi_2Te_4/Bi_2Te_3$ superlattice antiferromagnetic topological insulator, Sci. Bull. **65**, 2086 (2020).

[36] Y. Zhao and Q. Liu, Routes to realize the axion-insulator phase in $MnBi_2Te_4(Bi_2Te_3)_n$ family, Appl. Phys. Lett. **119**, 060502 (2021).

[37] M. M. Asmar, G. Gupta, and W.-K. Tse, Particle–hole asymmetry and quantum confinement effects on the magneto-optical response of topological insulator thin-films, J. Appl. Phys. **131**, 164305 (2022).

[38] X.-L. Qi, T. L. Hughes, and S.-C. Zhang, Topological field theory of time-reversal invariant insulators, Phys. Rev. B **78**, 195424 (2008).

[39] T. L. Hughes, E. Prodan, and B. A. Bernevig, Inversion-symmetric topological insulators, Phys. Rev. B **83**, 245132 (2011).

[40] Q. Niu, D. J. Thouless, and Y.-S. Wu, Quantized Hall conductance as a topological invariant, Phys. Rev. B **31**, 3372 (1985).

[41] R. Verresen, R. Moessner, and F. Pollmann, One-dimensional symmetry protected topological phases and their transitions, Phys. Rev. B **96**, 165124 (2017).

[42] J. E. Moore and L. Balents, Topological invariants of time-reversal-invariant band structures, Phys. Rev. B **75**, 121306(R) (2007).

[43] N. H. Lindner, G. Refael, and V. Galitski, Floquet topological insulator in semiconductor quantum wells, Nat. Phys. **7**, 490 (2011).

[44] H. Shen, B. Zhen, and L. Fu, Topological Band Theory for Non-Hermitian Hamiltonians, Phys. Rev. Lett. **120**, 146402 (2018).

[45] C. L. Kane and T. C. Lubensky, Topological boundary modes in isostatic lattices, Nat. Phys. **10**, 39 (2014).

[46] T. Ozawa, H. M. Price, A. Amo, N. Goldman, M. Hafezi, L. Lu, M. C. Rechtsman, D. Schuster, J. Simon, O. Zilberberg, and I. Carusotto, Topological photonics, Rev. Mod. Phys. **91**, 015006 (2019).

[47] F. Wu, T. Lovorn, and A. H. MacDonald, Topological Exciton Bands in Moiré Heterojunctions, Phys. Rev. Lett. **118**, 147401 (2017).

[48] Y. Onose, T. Ideue, H. Katsura, Y. Shiomi, N. Nagaosa, and Y. Tokura, Observation of the magnon Hall effect, Science **329**, 297 (2010).

[49] C.-X. Liu, S.-C. Zhang, and X.-L. Qi, The quantum anomalous Hall effect: Theory and experiment, Annu. Rev. Condens. Matter Phys. **7**, 301 (2016).

[50] C. L. Kane and E. J. Mele, Quantum Spin Hall Effect in Graphene, Phys. Rev. Lett. **95**, 226801 (2005).

[51] X. Wan, A. M. Turner, A. Vishwanath, and S. Y. Savrasov, Topological semimetal and fermi-arc surface states in the electronic structure of pyrochlore iridates, Phys. Rev. B **83**, 205101 (2011).

[52] A. A. Burkov and L. Balents, Weyl Semimetal in a Topological Insulator Multilayer, Phys. Rev. Lett. **107**, 127205 (2011).

[53] P. A. McClarty, Topological magnons: A review, Annu. Rev. Condens. Matter Phys. **13**, 171 (2022).

[54] G. Ma, M. Xiao, and C. T. Chan, Topological phases in acoustic and mechanical systems, Nat. Rev. Phys. **1**, 281 (2019).

[55] F. Harper, R. Roy, M. S. Rudner, and S. Sondhi, Topology and broken symmetry in Floquet systems, Annu. Rev. Condens. Matter Phys. **11**, 345 (2020).

[56] Z. Gong, Y. Ashida, K. Kawabata, K. Takasan, S. Higashikawa, and M. Ueda, Topological Phases of Non-Hermitian Systems, Phys. Rev. X **8**, 031079 (2018).

[57] X.-L. Qi, Y.-S. Wu, and S.-C. Zhang, Topological quantization of the spin Hall effect in two-dimensional paramagnetic semiconductors, Phys. Rev. B **74**, 085308 (2006).

[58] See Supplemental Material at http://link.aps.org/supplemental/10.1103/PhysRevB.108.045144 for further results for finite-size topology in Chern insulator models with Chern numbers 1 and 2, as well as details of disorder treatments, which includes Ref. [61].

[59] A. Alexandradinata, X. Dai, and B. A. Bernevig, Wilson-loop characterization of inversion-symmetric topological insulators, Phys. Rev. B **89**, 155114 (2014).

[60] K.-T. Chen and P. A. Lee, Unified formalism for calculating polarization, magnetization, and more in a periodic insulator, Phys. Rev. B **84**, 205137 (2011).

[61] D. Sticlet, F. Piéchon, J.-N. Fuchs, P. Kalugin, and P. Simon, Geometrical engineering of a two-band Chern insulator in two dimensions with arbitrary topological index, Phys. Rev. B **85**, 165456 (2012).